Locking depths estimated from geodesy and seismology along the San Andreas Fault System: Implications for seismic moment release

Bridget R. Smith-Konter,[1] David T. Sandwell,[2] and Peter Shearer[2]

Received 23 November 2010; revised 18 February 2011; accepted 24 February 2011; published 3 June 2011.

[1] The depth of the seismogenic zone is a critical parameter for earthquake hazard models. Independent observations from seismology and geodesy can provide insight into the depths of faulting, but these depths do not always agree. Here we inspect variations in fault depths of 12 segments of the southern San Andreas Fault System derived from over 1000 GPS velocities and 66,000 relocated earthquake hypocenters. Geodetically determined locking depths range from 6 to 22 km, while seismogenic thicknesses are largely limited to depths of 11–20 km. These seismogenic depths best match the geodetic locking depths when estimated at the 95% cutoff depth in seismicity, and most fault segment depths agree to within 2 km. However, the Imperial, Coyote Creek, and Borrego segments have significant discrepancies. In these cases the geodetically inferred locking depths are much shallower than the seismogenic depths. We also examine variations in seismic moment accumulation rate per unit fault length as suggested by seismicity and geodesy and find that both approaches yield high rates (1.5–1.8 × 10^{13} Nm/yr/km) along the Mojave and Carrizo segments and low rates (~0.2 × 10^{13} Nm/yr/km) along several San Jacinto segments. The largest difference in seismic moment between models is calculated for the Imperial segment, where the moment rate from seismic depths is a factor of ~2.5 larger than that from geodetic depths. Such variability has important implications for the accuracy to which future major earthquake magnitudes can be estimated.

Citation: Smith-Konter, B. R., D. T. Sandwell, and P. Shearer (2011), Locking depths estimated from geodesy and seismology along the San Andreas Fault System: Implications for seismic moment release, *J. Geophys. Res.*, *116*, B06401, doi:10.1029/2010JB008117.

1. Introduction

[2] Fault depth within the seismogenic zone is a critical parameter for seismic hazard models. Earthquake moment is proportional to the rupture area of a brittle fault, defined as the product of a fault's length and width (i.e., depth for a vertical fault). Major earthquakes ($M_o > 8$) have been shown to rupture the entire brittle fault zone [*Das and Scholz*, 1983; *Hill et al.*, 1990] and recent studies of seismicity using relocated hypocenters in Southern California [*Nazareth and Hauksson*, 2004] show that the depth above which 99% of the moment release of background seismicity occurs provides a realistic estimate of the maximum rupture depth in moderate to large earthquakes. Thus accurate estimates of maximum fault depth are fundamental in accurately forecasting the magnitude of future earthquakes.

[3] Geophysical observations from both seismology and geodesy can provide estimates of the fault depth. Earthquake hypocenters (Figure 1a) define a depth range of active seismicity within the crust, representing a transition from seismic faulting (velocity weakening) to aseismic slip (velocity strengthening) [*Brace and Byerlee*, 1970; *Marone and Scholz*, 1988]. While the average thickness of the seismogenic zone for the San Andreas Fault System (SAFS) is fairly shallow at ~12 km, large variations from less than 10 km in the Salton Trough area to greater than 25 km at the southwestern edge of the San Joaquin Valley have been identified [*Nazareth and Hauksson*, 2004]. Similarly, the seismogenic thickness of the SAFS can vary significantly along strike [e.g., *Peterson et al.*, 1996; *Magistrale*, 2002; *Wdowinski*, 2009]. These estimates of seismogenic thickness and fault segment length (i.e., slip area), combined with estimates of long-term fault slip rate, have been used to estimate the earthquake potential of faults along the SAFS [*Stein*, 2008].

[4] Geodetic surface deformation measurements (i.e., GPS (Figure 1b) or InSAR), combined with a mathematical model, can be used to estimate the effective thickness of the zone of interseismic strain accumulation, commonly referred to as the fault locking depth. The simple elastic dislocation model [*Savage and Burford*, 1973] describes the accumulation of elastic strain along a vertical strike-slip fault. The 2-D model velocity profile across the locked fault zone is given by

$$v(x) = \frac{V}{\pi}\tan^{-1}\frac{x}{D}, \quad (1)$$

[1]Department of Geological Sciences, University of Texas at El Paso, El Paso, Texas, USA.
[2]Institute for Geophysics and Planetary Physics, Scripps Institution of Oceanography, University of California, San Diego, La Jolla, California, USA.

0148-0227/11/2010JB008117

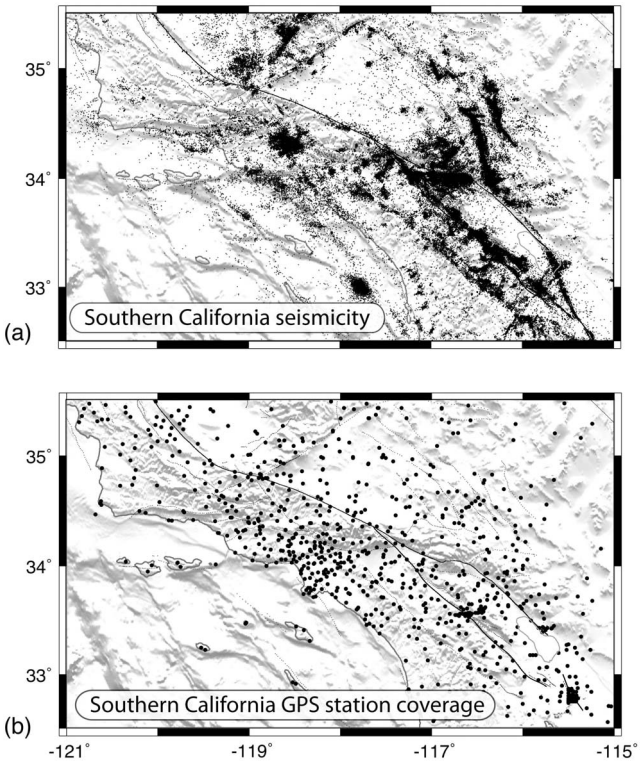

Figure 1. (a) Relocated seismicity for Southern California from 1981 to 2005 [from *Lin et al.*, 2007]. (b) Southern California EarthScope Plate Boundary Observatory GPS station locations. An additional high-density GPS array [*Lyons et al.*, 2002] straddling the Imperial fault was also combined with the EarthScope data set to provide additional coverage.

where V is the far-field velocity, x is the horizontal fault-perpendicular distance, and D is the locking depth (Figure 2 with $d = 0$). The actual variation of slip with depth is probably a gradual transition rather than an abrupt step and physical models can be easily modified to simulate a gradual transition. However, it has been demonstrated that the exact shape of this transition with depth cannot be resolved using surface geodetic data [*Savage*, 2006]. Moreover, for earthquake moment assessment, it is the effective thickness of the locked zone that is of interest, so the shape of the depth transition is irrelevant for this application and most investigators simply solve for the locking depth.

[5] The derivative of the velocity profile across the fault is the shear strain rate $\dot{\varepsilon}$. The peak strain rate occurs directly above the fault and has an amplitude given by

$$\dot{\varepsilon} = \frac{V}{\pi D}. \tag{2}$$

[6] Another related parameter is the seismic moment accumulation rate per unit fault length given by

$$\frac{\dot{M}}{L} = \mu V D, \tag{3}$$

where μ is the crustal shear modulus. Both strain rate and moment accumulation rate are important for assessing earthquake hazard. Strain rate multiplied by the shear modulus and the time since the last major rupture provides a first-order estimate of the stress that has accumulated since the last earthquake. While several studies have shown that earthquakes do not follow a characteristic rupture cycle [*Weldon et al.*, 2004], the accumulated stress is still a quantitative measure of whether a particular fault is early or late in its earthquake cycle. The seismic moment accumulation rate, however, is a more important measure of earthquake potential since this rate multiplied by the time since the last major rupture and the length of a potential rupture is a proven measure of earthquake size [*Stein*, 2008]. Since both strain rate and moment accumulation rate depend on slip rate and locking depth, or the thickness of the locked zone if the fault has shallow fault creep, understanding how these parameters are estimated and how they are applied in models is an important exercise.

[7] In this study we compare the effective thickness of the locked zone derived from seismicity with the thickness derived from geodesy to quantitatively measure the similarities and differences in the two approaches along the SAFS. Seismogenic thickness is derived from 66,775 earthquake epicenters [*Lin et al.*, 2007] and fault locking depths are estimated from 1099 GPS velocities for 12 fault segments. We examine variations in seismic moment accumulation rate along the fault system as suggested by seismicity and geodesy. Finally, we explore plausible explanations for fault depth discrepancies and examine the associated strengths and weaknesses of each method.

2. Locking Depth Estimated From Geodesy

[8] GPS velocity measurements can be used to estimate both the strain and moment accumulation rate. As described above, the key model parameters are the far-field velocity V and the locking depth D. An accurate estimate of the far-field velocity requires GPS velocity data more than several locking depths away from the fault (>50 km), while an accurate estimate of the locking depth requires a high density of GPS velocity data within one-half locking depth of the fault

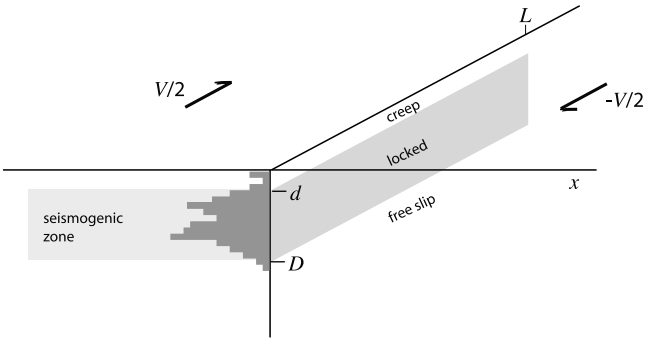

Figure 2. Diagram of a strike-slip fault of length L that is locked to depth D. The far-field slip rate is V. Some faults also have shallow fault creep to depth d, which reduces the effective thickness of the locked zone to $D - d$. The locked zone is sometimes equated to the seismogenic zone where the fault behavior is velocity weakening [*Marone and Scholz*, 1988]. Darker shading represents a hypothetical distribution of seismicity versus depth.

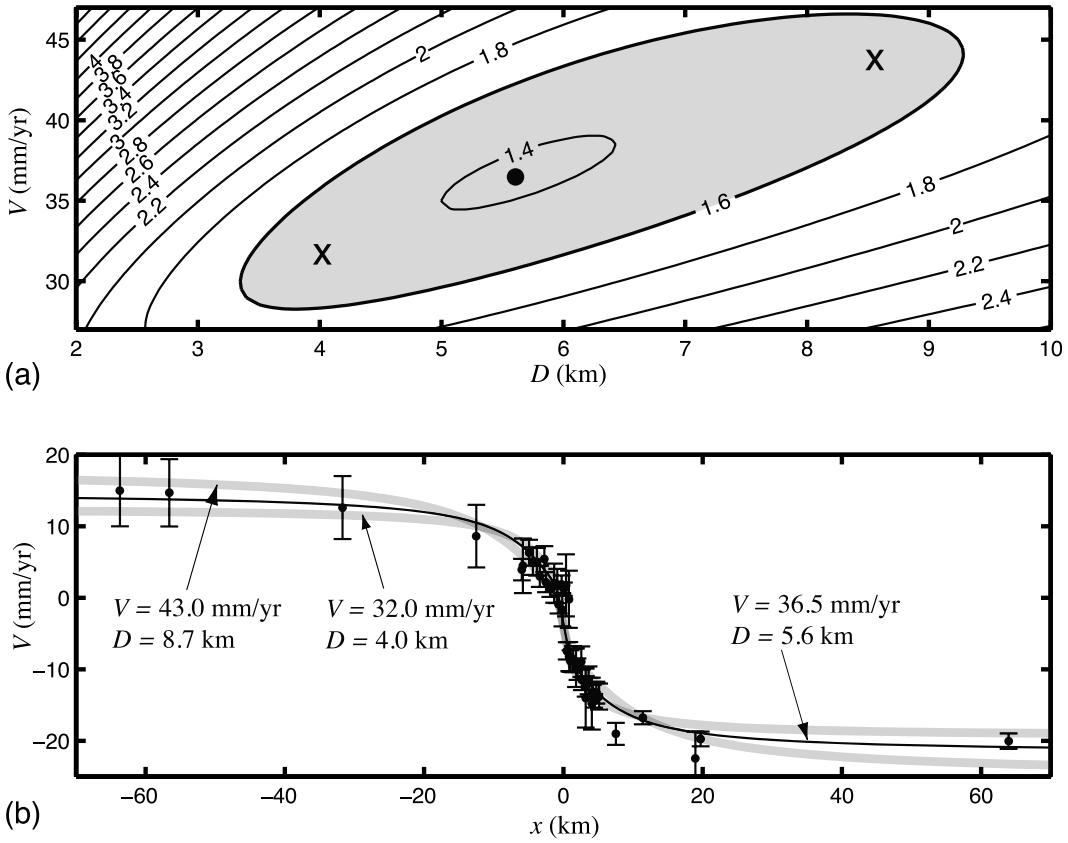

Figure 3. Bounds on best fitting two-dimensional dislocation models for dense GPS velocity measurements across the Imperial fault [*Lyons et al.*, 2002]. All models include 9 mm/yr of creep for depths less than 3 km. (a) Chi-square misfit versus deep locking depth D and far-field slip rate V shows the high degree of correlation between these two parameters. The crosses mark the bounds of the acceptable models plotted in Figure 3b. (b) Fault-perpendicular model profiles showing the best fitting model (locking depth of 5.6 km and slip rate of 36.5 mm/yr) and a sample of acceptable models (locking depths between 4 (32 mm/yr) and 8.7 km (44 mm/yr)).

(<6 km spacing). However, the typical spacing of GPS velocity measurements along the SAFS (Figure 1b) is only 10–20 km [*Wei et al.*, 2010]. Because of sparse geodetic data in some locations, depth uncertainties can be on the order of 3–6 km. Some faults also exhibit evidence of shallow fault creep [*Bürgmann et al.*, 2000; *Lyons et al.*, 2002] which reduces the effective width of the locked zone and can further complicate estimations of locking depth. In addition, real fault geometry is not simply two-dimensional and so the 3-D inversion for both slip rate and locking depth is usually ill conditioned [*McCaffrey*, 2005].

[9] A simple 2-D inversion example illustrates both issues of shallow creep and the ill conditioning of the slip rate and locking depth parameter estimation problem. We consider the case of the Imperial fault where there is a single fault strand with better than average spatial sampling owing to a dense GPS array above the fault zone (Figure 3). The first issue is that this fault has known shallow creep [*Goultry et al.*, 1978; *Genrich et al.*, 1997; *Lyons et al.*, 2002]. A least squares sensitivity analysis by *Lyons et al.* [2002] showed that the near-fault creep is explained by a shallow locking depth d of 3 km and a creep rate of 9 mm/yr. Moreover, they showed that the important lumped parameter is the effective thickness of the locked zone or $D - d$. Given these shallow fault creep parameters, we calculate the chi-square misfit of the simple arctangent model versus locking depth and slip rate (Figure 3). The contours of misfit are elongated, showing a high correlation between slip rate and locking depth. The best fit model has a slip rate of 36.5 mm/yr and a locking depth of 5.6 km, although models with locking depths between 4 and 8.7 km and slip rates between 32 and 43 mm/yr are acceptable. A model with a shallow locking depth of 4 km requires a low slip rate of 32 mm/yr, while a model with a deep locking depth of 10 km requires a slip rate of 44 mm/yr. This correlation between locking depth and slip rate has been demonstrated in several previous publications. For example, *Segall* [2002] showed a similar result for the Carrizo segment of the SAF and suggested that geological bounds on slip rate could be used to place bounds on the locking depth.

[10] In general, there are two practical approaches to estimating slip rate and locking depth from sparse geodetic data. Both start with a segmented representation of the fault system and use an elastic half-space or layered viscoelastic model to estimate crustal velocities at GPS sites. The standard approach is to fix the locking depth and invert for the slip rate or degree of coupling [*Becker et al.*, 2004; *Meade and Hager*, 2005a; *McCaffrey*, 2005]. The assumed locking depth (typically a constant 12, 15, or 20 km) is based on previous geo-

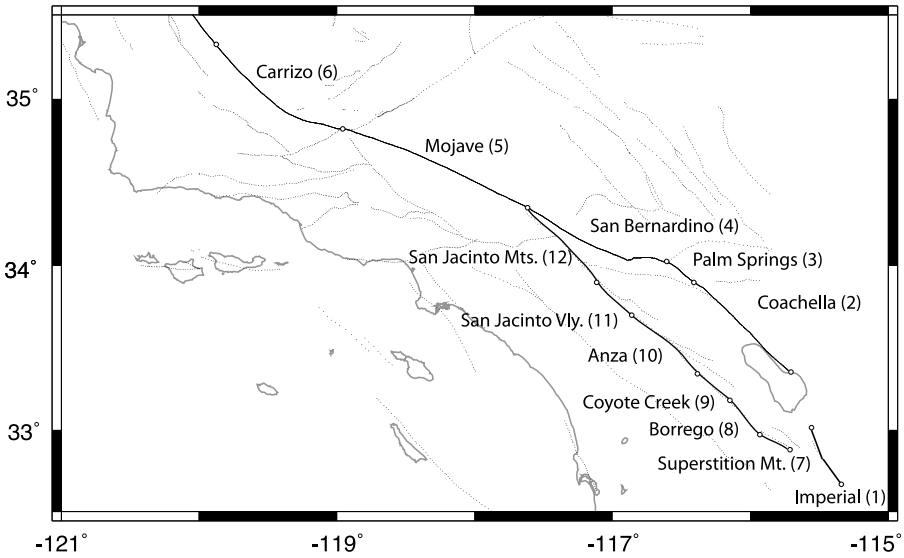

Figure 4. Fault location map of the southern San Andreas Fault System. Segment names and numbers correspond to those in Table 1.

detic studies or the average thickness of the seismogenic zone approximated from relocated earthquakes. An alternate approach is to fix the slip rate to the long-term rates assembled from numerous geological studies and invert for the locking depth along each segment [*Smith and Sandwell*, 2003]. Neither approach is completely satisfactory. In particular, if there are significant variations of 5–10 km in locking depth, then an approach using a fixed locking depth will result in estimates of slip rate that are significantly different (lower) than the true rate. For example, *Meade and Hager* [2005a] used a locking depth of 15 km for the San Bernardino segment of the SAF and found the best fit slip rate was only 5.1 ± 1.5 mm/yr, which is significantly less than the geologic estimate of 23–25 mm/yr [*Weldon and Sieh*, 1985]. *Smith-Konter and Sandwell* [2009] found an acceptable fit to the geodetic data using a slip rate of 16 mm/yr and a locking depth of 21 km. A third approach, not yet considered in any geodetic study, is to use variable depths from microseismicity as a proxy for the base of the locked zone.

[11] In this study we establish spatial variations in locking depth along 12 main segments of the southern SAFS (Figure 4) using a geodetically constrained semianalytic dislocation model [*Smith and Sandwell*, 2003, 2006; *Smith-Konter and Sandwell*, 2009]. Fault segments include Imperial (1), Coachella (2), Palm Springs (3), San Bernardino (4), Mojave (5), Carrizo (6), Superstition Mountains (7), Borrego (8), Coyote Creek (9), Anza (10), San Jacinto Valley (11), San Jacinto Mountains (12) (Table 1). In addition to these main segments, the total model (spanning 1000 × 1700 km in the east-west and north-south directions) consists of 42 vertical fault segments imbedded in an elastic plate overlying a viscoelastic half-space. Parameters and additional details for this model are provided in the work of *Smith-Konter and Sandwell* [2009]. Deep slip is prescribed along each of the major fault segments, which drives the secular interseismic crustal block motions. Slip rates are largely derived from geological studies [*Working Group on California Earthquake Probabilities* (*WGCEP*), 1995, 2003, 2007], which are incorporated into the model such that the cumulative slip rate across paralleling faults is constant. Fault segments are locked from the surface down to a variable locking depth, D, which is tuned to match the present-day GPS measurements.

[12] The relationship between surface velocity and locking depth is nonlinear, thus we estimate the depths using an iterative, least squares approach based on the Gauss-Newton method [cf. *Smith and Sandwell*, 2003]. The locking depth is varied along each fault segment to minimize the weighted-residual misfit to 1099 EarthScope Plate Boundary Observatory (PBO) GPS-derived horizontal velocities. This method searches the parameter space for optimal combinations of locking depths for all fault segments defined in the model. Uncertainties in estimated locking depths (1σ standard deviation) are determined from the covariance matrix of the final inversion iteration. Locking depth results are provided in Table 1. In a few special cases where recent single-fault segment investigations of locking depth are available and the fault is nearly two-dimensional [i.e., *Lyons et al.*, 2002], we adopt these estimates and adjust the uncertainty to reflect the range of results.

[13] Geodetically determined locking depths for the southern SAFS range from 5.9 to 21.5 km, with a mean of 13.9 km and a standard deviation of 5.7 km. Uncertainties in locking depth are typically 1 to 3 km, depending on the density and quality of nearby geodetic observations. Lower uncertainties are estimated along the Coachella and Mojave segments (0.5 and 0.4 km, respectively) where the EarthScope GPS array is quite dense (Figure 1b) and the velocity measurements have small errors. Larger uncertainties in locking depth occur along the Palm Springs and San Jacinto Valley segments (8 and 6.3 km, respectively). These fault segments are fairly complex and our simplified segmented model may not capture their complex deformation. Note also, we assign geologic slip rates of 23 and 12 mm/yr for the Palm Springs and San Jacinto Valley segments, respectively; however, slip rates for both of these segments are also highly contested [*Sharp*, 1981; *Weldon and Sieh*, 1985; *Bird and Kong*, 1994;

Table 1. Geodetic Locking Depth Estimates From This Study and Seismogenic Thickness Estimates From *Lin et al.* [2007] and *Nazareth and Hauksson* [2004][a]

Segment Number	Segment Name	Geologic Slip Rate (mm/yr)	Geodetic Depth (km)	Seismic Depth[b] (km)			Seismic Depth[c] (km)
				90%	95%	99%	
1	Imperial	40	5.9[d] +/− 3.0	10	10.8	14.4	15.6
2	Coachella	25	11.5 +/− 0.5	8.1	9.3	14.1	15.0
3	Palm Springs	23	16.4 +/− 8.0	11.4	12.3	15.3	19.4
4	San Bernardino	16	17.8 +/− 2.0	16.1	17.5	19.6	20.7
5	Mojave	33	16.8 +/− 0.4	12.6	13.3	14.4	13.2
6	Carrizo	36	18.7 +/− 2.0 16.7[e] +/− 2.2	13.9	14.4	16.0	17.5
7	Superstition Mountain	15	10.8 +/− 1.1	10.2	10.7	12.6	12.0
8	Borrego	15	6.4 +/− 1.4	10.7	11.4	13.5	13.9
9	Coyote Creek	15	6.3 +/− 2.0	13.2	13.6	14.5	16.4
10	Anza	15	13.7 +/− 3.2	15.8	16.5	17.9	20.0
11	San Jacinto Valley	12	21.5 +/− 6.3	17.1	17.5	18.9	19.6
12	San Jacinto Mountains	12	21.0 +/− 3.2	17.0	17.5	18.6	19.4

[a]Estimates from *Lin et al.* [2007] are provided at maximum depths spanning 90%, 95%, and 99% of the total seismicity.
[b]From *Lin et al.* [2007].
[c]From *Nazareth and Hauksson* [2004].
[d]With 3 km of shallow creep included [*Lyons et al.*, 2002].
[e]Mean and standard deviation of locking depth estimated from nine independent analyses of the same geodetic data set for the UCERF-3 Workshop exercise; see http://www.scec.org/workshops-/2010/gpsucerf3-Report_on_2010_SCEC_GPS_UCERF3-_Workshop_v2.pdf.

Becker et al., 2004; *Meade and Hager*, 2005a]. A trade-off in slip rate between the parallel strands of the San Andreas and San Jacinto faults has been suggested [*Bennett et al.*, 2004] and our model likely requires an adjusted slip rate in this region to provide tighter constraints on the locking depth over variable timescales.

[14] The dense GPS array at the Imperial fault (Figure 5a) illustrates the issues with shallow creep, showing that geodesy only estimates the thickness of locked zone. Published values of locking depth for the Imperial fault range from 6 to 13 km [*Archuleta*, 1984; *Genrich et al.*, 1997; *Lyons et al.*, 2002; *Smith and Sandwell*, 2003], typically accompanying 35–40 mm/yr of slip. However, the Imperial fault is known to exhibit fairly complex slip behavior with associated creep and perhaps cannot be accurately modeled as a single fault segment that is simply locked at depth. Our 3-D locking depth inversion is 5.5 km, which includes 3 km of shallow creep. Because the Imperial fault is nearly straight, this 3-D inversion corresponds to the 2-D estimate shown in Figure 3.

[15] As this approach of using geologically derived slip rates to estimate locking depth is unique to our work, analyses by other groups are needed to relate our formal uncertainties in locking depth to the range of locking depths derived using other methods. Recently, the Southern California Earthquake Center (SCEC) hosted a workshop to evaluate the role of geodetic data for updating the Unified California Earthquake Rupture Forecast Version 3 (UCERF3; see http://www.scec.org/workshops-/2010/gpsucerf3-Report_on_2010_SCEC_GPS_UCERF3-_Workshop_v2.pdf and *Smith-Konter et al.* [2010]). One of the exercises (E. Hearn, personal communication, 2010) was to fit the geodetic data across the Carrizo segment of the SAF using whatever method investigators felt was most appropriate. Six investigators participated in this exercise using nine different modeling approaches ranging from simple elastic half-space back slip models to full numerical analyses using nonlinear time-dependent rheology. Remarkably, all of the analyses provided roughly the same locking depth solution (16.7 ± 2.2 km), suggesting that the derived value is largely independent of the method or investigator. These 9 values disagree with older published models with a 25 km locking depth [*Eberhart-Phillips et al.*, 1990], suggesting that newer campaign data provided by the USGS and EarthScope have helped refine the locking depth for this segment. Slip rates along this region are reasonably well constrained (i.e., 36 mm/yr; see *Schmalzle et al.* [2006]). Our estimate of locking depth for the Carrizo segment of 18.7 +/− 2.0 km (Figure 5b) is on the higher end of the 6 analyses but still within one standard deviation of the range of estimates. On the basis of this comparison of results, we believe that our geodetic estimates are accurate and the uncertainties depend on both the near-fault data distribution and 3-D geometry.

3. Seismogenic Thickness Estimated From Seismicity

[16] A number of studies have examined the maximum depth of seismicity in different regions in California and related the results to differences in heat flow, rock type, and main shock rupture models [*Doser and Kanamori*, 1986; *Miller and Furlong*, 1988; *Sanders*, 1990; *Williams*, 1996; *Magistrale and Zhou*, 1996; *Richards-Dinger and Shearer*, 2000; *Bonner et al.*, 2003; *Nazareth and Hauksson*, 2004]. In general, these results depend upon the quality of the earthquake locations and the choice of a cutoff criteria used to define the maximum depth. To achieve robust depth estimates that are insensitive to occasional stray earthquake locations at large depth, most studies have assigned a cutoff percentile depth, which has ranged from 90% [*Miller and Furlong*, 1988; *Richards-Dinger and Shearer*, 2000], to 95% [*Williams*, 1996], to 99% [*Bonner et al.*, 2003]. A somewhat different approach was used by *Nazareth and Hauksson* [2004], who computed the 99.9% limit in total seismic moment (estimated from the local earthquake magnitudes for small earthquakes). This study (NH04, hereafter) used earthquakes relocated using a 3-D velocity model and found that the 99.9% moment limit in background seismicity reliably predicted the maximum rupture depth of moderate to large earthquakes in Southern California.

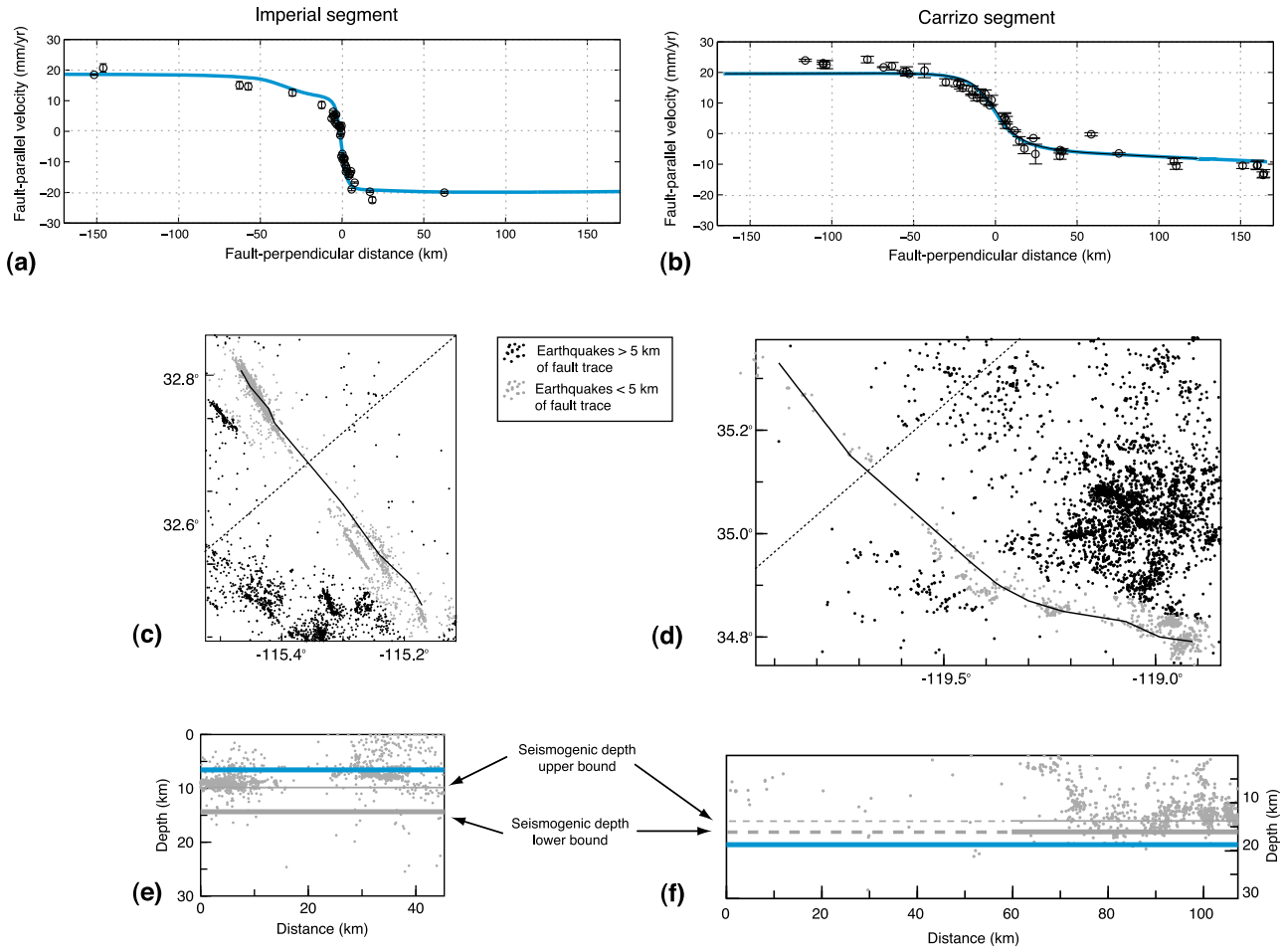

Figure 5. GPS velocities and seismicity for the Imperial and Carrizo segments. (a) Fault-parallel velocity of the Imperial fault segment as a function of fault-perpendicular distance. Profile location is shown in map view as a dashed line in Figure 5c. GPS velocities from stations located within a ~50 km perpendicular distance from the profile are shown as open circles, and the velocity model profile is shown in blue. (b) Same as Figure 5a for the Carrizo segment. Profile location is shown as a dashed line in Figure 5d. (c) Map view of seismicity along the Imperial fault from *Lin et al.* [2007]. Gray dots indicate earthquake locations within 5 km from the fault trace used in this study. (d) Same as Figure 5c for the Carrizo segment. (e) Seismicity as a function of depth along the Imperial fault trace. The blue line represents the geodetic locking depth estimate, and the thick gray line represents the 99% seismicity cutoff depth (lower bound) from the *Lin et al.* [2007] catalog. Also plotted are the upper bounds on seismogenic depth (thin gray line), representing the 90% seismicity cutoff depth. (f) Same as Figure 5e for the Carrizo segment. Dashed lines represent regions devoid of seismicity.

[17] Here we examine earthquake depths in the LSH catalog of *Lin et al.* [2007], which used waveform cross correlation and a new 3-D velocity model for Southern California to relocate over 400,000 earthquakes between 1981 and 2005 (Figure 1a). We examine seismicity profiles along the same fault segments used in our geodetic dislocation model, assuming vertical faults and including all earthquakes within 5 km (Figures 5c–5f). We calculate the 90%, 95% and 99% cutoff depths to see which best matches the geodetic data. We will refer to these results as LSH07.

[18] It should be noted that it is not always clear if the seismicity within 5 km of each fault segment is associated with the target fault. For example, seismicity along the southernmost SAF (segments 2 and 3) is relatively sparse and thus our locking depth estimates are largely based on the seismicity located about 4 to 5 km northeast of the surface trace of the fault. *Lin et al.* [2007] argue that this seismicity is likely on a northeast dipping SAF because this can explain geodetic data indicating that the maximum shear strain is displaced about 7 km northeast of the surface trace [*Fialko*, 2006]. However, the possibility also exists that the seismicity is on a parallel fault system to the SAF. Secondary faults could play a role for other fault segments as well, particularly for the complicated seismicity associated with many parts of the San Jacinto fault, the San Bernardino segment of the SAF, and where the White Wolf and Garlock faults approach the SAF. These differences could bias our results if these secondary faults have different locking depths and maximum

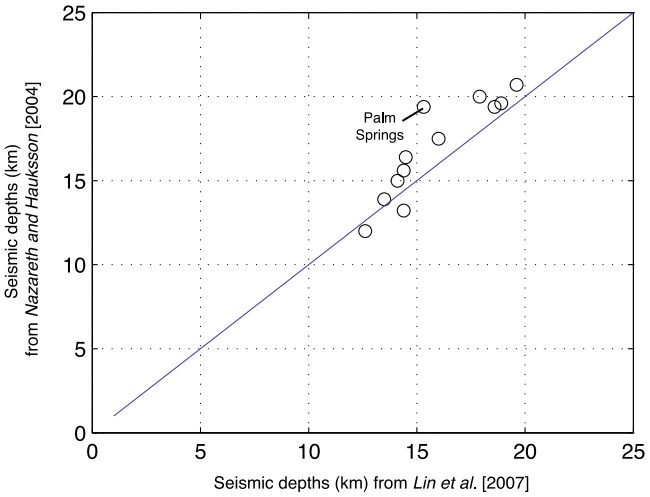

Figure 6. Comparison of seismogenic thickness (depths) estimated by *Lin et al.* [2007] (LSH07, 99% seismicity cutoff depth, horizontal axis) and *Nazareth and Hauksson* [2004] (NH04, vertical axis). Perfect agreement would follow the diagonal line. The largest outlier (segment 3) is the Palm Springs segment.

seismicity depths than the main fault. However, as we will show later, we generally observe a correlation between our measured maximum seismicity depth and geodetic locking depth for these segments, suggesting that any biases owing to off-fault seismicity are small.

[19] For the fault segments used in this study, seismicity evaluated by both NH04 and our LSH07 results suggests that the seismogenic thickness in Southern California is largely limited to the upper 11–20 km of the crust, with a mean thickness of 15.8 km and a standard deviation of 2.3 km (Table 1). We compute differences in seismogenic thickness estimates of NH04 (99.9% moment depth) and LSH07 (90%, 95%, and 99% depth) and find standard deviations of 2.13, 1.96, and 1.34 km, respectively. As expected, depths derived from a 99% seismicity cutoff depth provide the closest match to depths from NH04 (Figure 6). The NH04 estimates are slightly higher than those of LSH07 for most segments, suggesting that there may be some systematic differences in the earthquake depths in the two catalogs. The Palm Springs segment (3) has the largest disagreement in seismogenic thickness, where NH04 estimate it at 19.4 km and LSH07 estimate it at 15.3 km. The seismicity along this segment in map view is diffuse and a simple fault trace is not easily defined (Figure 1); the geographic coordinates of the segment location utilized in this study (combined with the LSH07 profiles) are approximated on the basis of our geodetic model constraints and we have likely oversimplified the horizontal fault geometry here. Overall though, the correlation of seismogenic thicknesses estimated by both studies is quite good.

4. Geodetic Locking Depth Versus Seismogenic Thickness

[20] Next we compare the locking depths inferred from geodetic models to seismogenic thickness derived from seismicity. The first issue is which of the cutoff percentages for the seismogenic depth best matches the geodetic locking depth. A regression analysis shows standard deviations of 4.20 km (90% seismicity, LSH07), 4.16 km (95% seismicity, LSH07), 4.30 km (99% seismicity, LSH07), and 4.60 km (99.9% moment, NH04). While the 95% seismicity LSH07 provides the best statistical match, the 99% seismicity LSH07 provides a better visual fit (Figure 7). Because there are many earthquakes for each segment, the formal standard errors associated with each cut-off depth percentage are very small. In Figure 7 we show the depth range spanned between the 90 to 99% depth estimates, which provides a more realistic picture of the likely depth uncertainties. Nine out of the twelve fault segments show agreement better than 2 km and the combined geodetic and seismic depth uncertainties for most of these segments overlap.

[21] Three outliers are evident from Figure 7 (Imperial (1), Coyote Creek (8), and Borrego (9)), which have significantly larger differences that are well outside the error bounds of the geodetic locking depths. In these cases the geodetic locking depths are much shallower than the seismogenic depths. By omitting these three outliers, the geodetic and seismic data agreement is significantly improved, with standard deviations of 2.38 km (90% seismicity, LSH07), 2.44 km (95% seismicity, LSH07), 2.68 km (99% seismicity, LSH07), and 3.22 km (99.9% moment, NH04). The generally good agreement between seismogenic thickness and geodetic locking depths suggests that both methods provide a reasonable estimate of the depth to the base of the locked zone to within

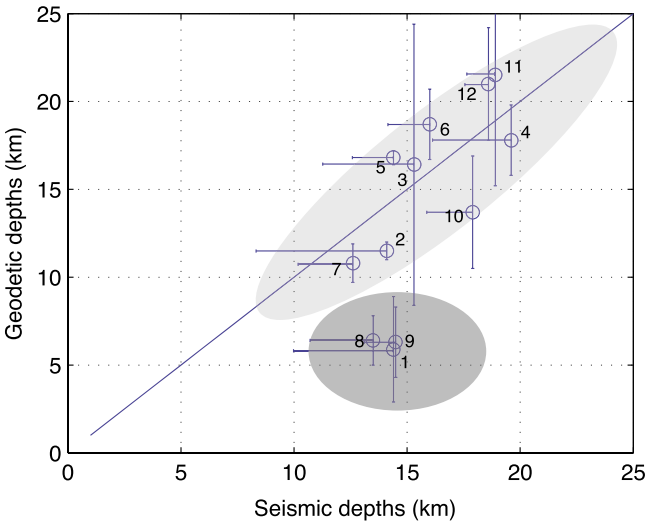

Figure 7. Comparison of seismogenic thickness (depths) estimated by LSH07 (99% seismicity cutoff depth, horizontal axis) and geodetic locking depths (vertical axis). Uncertainty estimates in geodetic depths (Table 1) and seismogenic depths (approximated from 90–99% seismicity cutoff depth estimates) are also plotted. Number labels correspond to segment numbers as in Table 1.The light shaded oval represents data that cluster around the 1:1 match in depths, represented by the diagonal line. The dark shaded circle represents outliers (segments 1, 8, and 9) where seismicity suggests much deeper fault locking depths than geodesy.

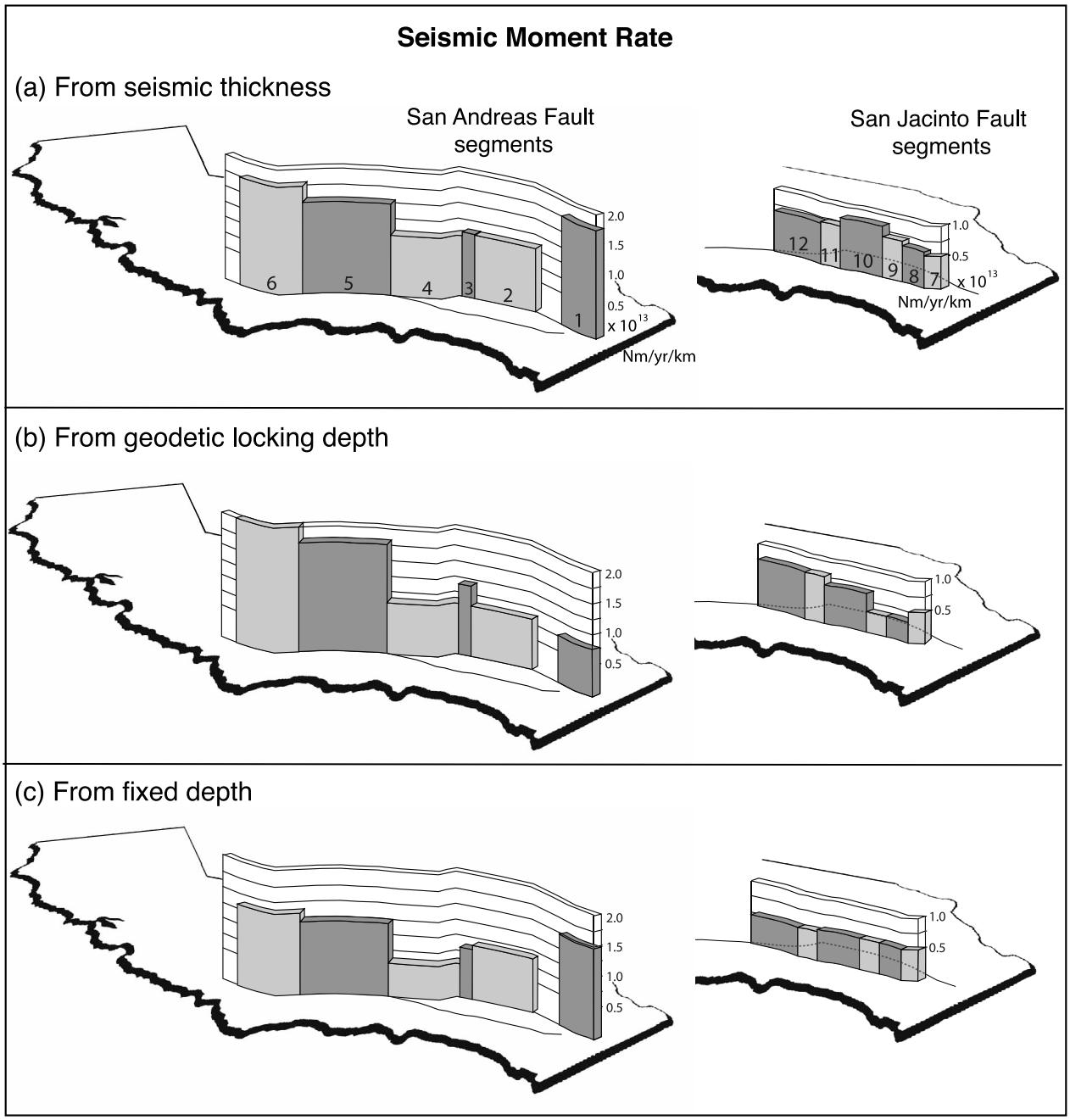

Figure 8. Seismic moment rate per unit length, assuming depths (a) derived from seismic thickness, (b) derived from geodetic locking depth, and (c) set to a fixed depth of 12 km. Perspective plots on the left are for the San Andreas Fault segments (labeled 1–6 in Figure 8a), while plots on the left represent segments of the San Jacinto fault (labeled 7–12 in Figure 8a).

a mean accuracy of 2.5 km when the three significant outliers are excluded.

5. Seismic Moment Rate

[22] Using equation (3), we calculate seismic moment accumulation rate per unit length for each fault segment of the SAFS using both seismically and geodetically derived locking depths (Figure 8). Here we assume a constant shear modulus of μ = 30 GPa and adopt slip rates according to Table 1. The highest rates of seismic moment accumulation from seismicity (1.5–1.8 × 10^{13} Nm/yr/km) occur along the Mojave, Carrizo, and Imperial segments, where seismic depths are moderately deep (14–16 km) and the slip rates are high (33–40 mm/yr). Similarly, moment rate estimates from geodesy are also highest along the Mojave and Carrizo segments, although not along the Imperial segment owing to the smaller geodetic locking depth estimated there (6 km). The lowest seismic moment rates (~0.2 × 10^{13} Nm/yr/km) for both models occur along the San Jacinto segments of Borrego

and Coyote Creek where the locking depth is shallower (~6 km) and the slip rates are 12–15 mm/yr.

6. Discussion

[23] As previous studies have demonstrated, microseismicity along the SAFS shows significant variations in seismogenic depth, ranging between 10 and 25 km [*Nazareth and Hauksson*, 2004]. Our geodetic analysis yields a slightly larger depth range of 6 to 22 km. This relative agreement suggests that these variations in fault depth are real. Distributions of fault depths can be attributed to both geological and geophysical factors, such as crustal temperature and lithology [e.g., *Miller and Furlong*, 1988; *Magistrale and Zhou*, 1996; *Magistrale*, 2002; *Bonner et al.*, 2003]. These studies suggest an inverse correlation between maximum depth of seismicity and heat flow along the southern SAF, and our estimates of depth, both seismic and geodetic, are consistent with these results. High heat flow values (~100 mW/m^2; see *Blackwell and Steele* [1992]) and shallow depths (6–10 km) are found in the Imperial Valley, which is characterized by thick sediments and young mafic igneous rocks [*Fuis et al.*, 1982; *Lachenbruch et al.*, 1985; *Magistrale*, 2002]. Alternatively, some of the lowest heat flow values in this region (~60 mW/m^2) and deeper locking depths (18–21 km) are found in granitic rocks along the San Gorgonio Pass, straddling the San Bernardino and San Jacinto Valley/Mountains segments [*Magistrale*, 2002].

6.1. Seismic and Geodetic Depth Discrepancies

[24] The three significant outliers (1, Imperial; 8, Coyote Creek; and 9, Borrego) all have geodetic locking depths that are much less than the seismogenic depths. Of course the creeping segment of the San Andreas Fault is the most notable example of this behavior, since the microseismicity extends to a depth of ~7–9 km [*Bedrosian et al.*, 2004] while the thickness of the geodetic locked zone is essentially zero [*Savage and Burford*, 1973; *Thatcher*, 1979]. A recent study of the San Jacinto fault zone (including both the Coyote Creek and Borrego segments) arrives at the same conclusion that the seismogenic depth is much greater than the thickness of the geodetically derived locked zone [*Wdowinski*, 2009]. Creep rates of ~5 mm/yr have been observed along the southern San Jacinto fault [*Louie et al.*, 1985]; however, radar interferometry [*Vincent*, 1998; *Lyons and Sandwell*, 2003] shows no evidence for shallow creep except along the southernmost Superstition Mountain segment where the slip occurs in episodes with a mean rate of 3 mm/yr [*Wei et al.*, 2010]. The largest outlier is the Imperial fault where the geodetic locking depth is only 6 km and the seismogenic depth is 14 km. This is a case where geodetically determined depths track middle-depth clusters of seismicity (~5–10 km; see Figure 5e). As previously discussed, the Imperial segment is known to exhibit both locked fault and creeping deformation behaviors with depth [*Lyons et al.*, 2002; *Shearer*, 2002], which appear to complicate both geodetic and seismic estimates of the thickness of the locked zone.

[25] It is possible that discrepancies in seismic and geodetic depths are revealing time-varying stress adjustments at depth throughout the earthquake cycle. If a recent earthquake has occurred on a fault segment, microseismicity can reflect a redistribution of stress within the fault zone. Outlier segments 1 and 9 have had relatively recent earthquakes (Imperial, 1940 and 1979; Borrego, 1968). In particular, aftershocks in the first 2 months following the M6.6 1979 Imperial Valley earthquake were 2–3 km deeper than premain shock seismicity [*Doser and Kanamori*, 1986]. Similar behavior was observed for the 1992 M7.3 Landers earthquake [*Rolandone et al.*, 2004] where aftershock depths deepened from pre-earthquake levels by as much as 3 km over 4 years. Thus it is possible that deeper distributions of seismicity along historically active faults of the SAFS can be attributed to post-seismic stress adjustments. Earthquake cycle effects are also known to complicate geodetic estimations of true locking depth [*Savage*, 1990; *Meade and Hager*, 2004], where fault locking depths tend to deepen nearing the end of an earthquake cycle.

[26] We must also consider the possibility that some of the differences in depth may be explained by along-strike variations in slip mechanisms, such as patches of vertical creeping between locked regions. The Parkfield segment north of our study area is known to exhibit such localized slip variations [*Harris and Segall*, 1987; *Werner et al.*, 1997; *Murray et al.*, 2001]. Combined with the long-wavelength along-strike variations in depth along the entire SAFS, it is certainly possible that individual fault segments may have small vertical creeping patches that are unaccounted for here. The impact of along-strike creeping patches on geodetic depths depends on the assigned fault segment length, and if a segment were to exhibit a significant span of creep along-strike, then geodetic measurements straddling such a region should yield a shallower depth than a fault segment that was strictly locked along strike.

[27] Recent evidence of nonvolcanic tremor has also been linked to vertical transition zones from fault locking to aseismic slip [*Obara et al.*, 2004; *Rogers and Dragert*, 2003]. While nonvolcanic tremor has been identified in six regions in California to date [*Nadeau and Dolenc*, 2005; *Gomberg et al.*, 2008], the only known tremor location relevant to this study is along the San Jacinto Valley segment near Hemet, CA. Here tremor depths, although poorly constrained, are estimated at 12 km depth [*Gomberg et al.*, 2008]. This depth is much shallower than the geodetic depth (21 km) and the 99% seismicity cutoff depth (19 km) determined for this segment. There is no evidence of shallow fault creep along this fault segment, but perhaps deeper aseismic slip is taking place here, as has been suggested for fault segments to the south of this segment along the San Jacinto fault [*Wdowinski*, 2009].

6.2. Fault Geometry

[28] This analysis assumes that the fault depth is constant with each predefined fault segment strike. How realistic is this assumption? Both geodetic and seismic estimates presented here are basically an along-strike average of the data sampled. Since geodetic estimates are model dependent and require a complicated segmentation scheme to provide sufficient along-strike resolution to address realistic variations, some guidance is provided by the seismicity. Significant along-strike variations in fault depth are evident in the seismic record, where for example, the San Bernardino segment has a maximum depth of seismicity that is much deeper in the

south (~20 km) than in the north (10–15 km) [*Magistrale and Zhou*, 1996; *Richards-Dinger and Shearer*, 2000, Plate 6; *Nazareth and Hauksson*, 2004]. Such variations may be due to reverse faulting in the structurally complex area along the San Gorgonio Pass [*Yule and Sieh*, 2003]. In this study we segment sections of the SAF consistent with our geodetic analysis, which follows previous segmentation schemes by *WGCEP* [1995, 2007] and *Plesch et al.* [2007]. In particular, we treat most of the San Bernardino segment as one estimate. NH04 considered this issue and evaluated seismic depths on a 5 km scale, in addition to an along-strike average. For the San Bernardino segment, for example, the 5 km segmentation and the along-strike average have depth differences of about 3 km. Geodetic determination of locking depth requires a dense array of stations within <6 km of a fault (across-strike), and while this is available along some fault segments (e.g., Imperial), it is not feasible for the entire system so the segmentation must be rather coarse. This coarse segmentation does not always capture the transition from locked to unlocked faults. Nevertheless, locking depth estimates from geodesy do provide realistic locking depths in regions where microseismicity is relatively scarce (i.e., Death Valley, Eastern California Shear Zone).

[29] Dipping fault geometry may also play an important role in understanding discrepancies between geodetic and seismic fault depths. While the orientations of most segments of the SAFS are assumed to be vertical (Community Fault Model; see http://structure.harvard.edu/cfm, *Plesch and Shaw* [2003], and *Plesch et al.* [2007]), some recent studies have suggested a variable degree of dip. Most notably, along the Carrizo and Coachella segments, fault dips are estimated between 55 and 75 degrees to the southwest and between 37 and 60 degrees to the northeast, respectively [*Lin et al.*, 2007; *Fuis*, 2007; Fuis et al., A new perspective on the geometry of the San Andreas Fault in Southern California and its relationship to lithospheric structure, submitted to *Bulletin of the Seismological Society of America*]. Fault dip has also been estimated for the Imperial fault at roughly 80 degrees to the east [*Reilinger and Larsen*, 1986]. Our geodetic model assumes a vertical dipping geometry for all fault segments of the SAFS, and this assumption may introduce an additional source of error when estimating fault depth. The fact that we observe seismic depths that are mostly a few kilometers deeper than geodetic depths follows the idea that a dipping fault would lengthen the geodetic locking depth. The largest discrepancy of fault depth, however, is largely derived from segments of the San Jacinto fault. Fault dip for segments of the San Jacinto fault are not well documented in the literature and the faults are typically assumed to be vertical. Inspection of the seismicity along the San Jacinto fault in map view also supports a vertical fault geometry, as the earthquake locations primarily align with the known mapped fault trace. The southernmost 15 km of the Coyote Creek fault segment, however, does show a clustering of seismicity to the southeast of the mapped fault trace, suggesting a dipping geometry may be relevant here.

6.3. Role of Fault Depth in Seismic Hazard Analyses

[30] These results have major implications for the seismic moment accumulation rate of segments of the SAFS. Moment accumulation rate is often calculated from observed rates of surface strain accumulation [*WGCEP*, 1995, 1999; *Ward*, 1994; *Savage and Simpson*, 1997] and typically evaluated for a constant locking depth of 10–15 km [*WGCEP*, 1995, *WGNCEP*, 1996; *Meade and Hager*, 2005b]. However, as our results clearly illustrate, seismic moment accumulation rates are very different when a constant locking depth of, for example, 12 km is adopted (Figure 8c). In this case, the largest moment accumulation rate occurs along the Imperial and Carrizo segments where the slip rate is largest (~37 mm/yr). The factor of 2 increase on the Imperial segment in comparison with geodetic depths (Figure 8b) reflects the factor of 2 increase in locking depth, while the 1/3 decrease in moment rate along the Carrizo segment is related to the 1/3 decrease in locking depth. The mean value of each group of seismic moment accumulation rates is also reflective of depth behavior: 0.99×10^{13} Nm/yr/km (seismic depths), 0.87×10^{13} Nm/yr/km (geodetic depths), and 0.77×10^{13} Nm/yr/km (constant D = 12 km). Moreover, we find that the main San Andreas Fault strand (including segments 1–6) accumulates roughly 67–70% of the seismic moment budget for all three models.

[31] The Uniform California Earthquake Rupture Forecast Version 2 (UCERF2) report [*WGCEP*, 2007] similarly recognizes the southern San Andreas as a region of elevated seismic potential. Overall, this study emphasizes the southern San Andreas (segments 2–6 here) as the region of most significant earthquake hazard in all of California, having a 59% probability of a $M \geq 6.7$ event over the next 30 years. *WGCEP* [2007] also determines a 31% probability for the San Jacinto segment (segments 7–12 here) and a 27% probability for the Imperial segment. For the faults included in our study, the UCERF2 report presents the highest "participation probability" of rupture occurrence for the Mojave and Carrizo segments of the San Andreas, consistent with the relatively higher seismic moment rates of these segments from both seismic and geodetic estimates (Figure 8). Conversely, UCERF2 segment rupture probabilities are highest along the Coachella segment, while this segment's calculated seismic moment rate is not unusually large; only when one accounts for the time elapsed since the last major earthquake event (300^{+} years) does the Coachella segment's accumulated seismic moment become significant. It is also important to note that depths utilized by the *WGCEP* [2007] for the UCERF2 report (which are largely based on maximum depths of background seismicity; see *Nazareth and Hauksson* [2004] and *Plesch et al.* [2007]) span a relatively small range, ~10–17 km, in comparison with the 6–22 km geodetic depth range presented here. While UCERF2 fault depths are sometimes larger than our geodetic depths (e.g., 15.9 km for Coyote Creek), relative shallower depths are also reported (e.g., 12.8 km for San Bernardino).

7. Conclusions

[32] In summary, this study of seismic and geodetic depths of the southern San Andreas Fault System has shown that maximum depths of seismicity largely agree with fault locking depths derived from geodetic models. Of the 12 fault segments analyzed here, we identify 3 outliers (Imperial, Coyote Creek, and Borrego segments) with significant (>8 km) seismic verses geodetic depth disagreements. For these segments, maximum seismicity depths are much larger

than geodetic locking depth estimates, suggesting that shallow creep or temporal variations in strain release throughout the earthquake cycle may contribute to these discrepancies.

[33] These results also highlight several important points that warrant further consideration. First, significant depth variations exist throughout the southern SAFS, bracketed by a range as large as 6 to 22 km. This result, combined with a statistical correlation between locking depth and slip rate, suggests that geodetically derived slip rates using models having fixed locking depths (i.e., 12 or 15 km) may be inaccurate. At least 7 of the 12 segments studied here have geodetic locking depths outside of the standard 12–15 km range. Furthermore, while geodetic depths indicate that 12 km is closer to the mean depth for segments of the southern SAFS, seismicity shows that 12 km might be a minimum faulting depth. This analysis also suggests that part of the disagreement between geodetically derived slip rates and geologically derived slip rates [e.g., *Weldon and Sieh*, 1985; *Meade and Hager*, 2005a] may be due in part to an incorrect assumption of a constant locking depth for fault segments. Moreover, when evaluating slip rates on faults, geodetic models should consider adopting variable depths from microseismicity to approximate the base of the locked zone.

[34] Finally, we urge future earthquake probability working groups and other independent seismic hazard analyses to consider depth variations reflected in geodetic models. Dense geodetic data sets (GPS and InSAR) are now available to further scrutinize fault locking depths of the SAFS. As demonstrated here, geodetic depths are largely consistent with maximum seismicity depths but provide a larger range of depth variations throughout the fault system. These depths can yield drastically different seismic moment rates for a single segment (in some cases, over a factor of 2), which should ultimately be reflected in earthquake probability forecasts.

[35] **Acknowledgments.** We thank Ross Stein and an anonymous reviewer for their helpful comments for improving this manuscript. We also thank Teira Solis for her assistance with figure graphics. This research was supported by the National Science Foundation (NSF; EAR0838252, EAR0811772, and EAR0847499), NASA (NNX09AD12G), and the Southern California Earthquake Center (SCEC). SCEC is funded by NSF Cooperative Agreement EAR-0106924 and USGS Cooperative Agreement 02HQAG0008. The SCEC contribution number for this paper is 1471.

References

Archuleta, R. J. (1984), A faulting model for the 1979 Imperial Valley earthquake, *J. Geophys. Res.*, *89*, 4559–4585, doi:10.1029/JB089iB06p04559.

Becker, T. W., J. Hardebeck, and G. Anderson (2004), Constraints on fault slip rates of the Southern California plate boundary from GPS velocity and stress inversions, *Geophys. J. Int.*, *160*, 634–650, doi:10.1111/j.1365-246.

Bedrosian, P. A., M. J. Unsworth, G. D. Egert, and C. H. Thurber (2004), Geophysical images of the creeping segment of the San Andreas Fault: Implications for the role of crustal fluids in the earthquake process, *Tectonophysics*, *385*, 137–158, doi:10.1016/j.tecto.2004.02.010.

Bennett, R. A., A. M. Friedrich, and K. P. Furlong (2004), Co-dependent histories of the San Andreas and San Jacinto fault zones from inversion of geologic displacement rate data, *Geology*, *32*, 961–964, doi:10.1130/G20806.1.

Bird, P., and X. Kong (1994), Computer simulations of California tectonics confirm very slow strength of major faults, *Geol. Soc. Am. Bull.*, *106*, 159–174, doi:10.1130/0016-7606(1994)106<0159:CSOCTC>2.3.CO;2.

Blackwell, D. D., and J. L. Steele (1992), The decade of North American geology, geothermal map of North America, scale 1:5,000,000, Geol. Soc. of Am., Denver.

Bonner, J. L., D. D. Blackwell, and E. T. Herrin (2003), Thermal constraints on earthquake depths in California, *Bull. Seismol. Soc. Am.*, *93*, 2333–2354, doi:10.1785/0120030041.

Brace, W. F., and J. D. Byerlee (1970), California earthquakes: Why only shallow focus?, *Science*, *168*, 1573–1575, doi:10.1126/science.168.3939.1573.

Bürgmann, R., D. Schmidt, R. M. Nadeau, M. d'Alessio, E. Fielding, D. Manaker, T. V. McEvilly, and M. H. Murray (2000), Earthquake potential along the northern Hayward fault, California, *Science*, *289*, 1178–1182, doi:10.1126/science.289.5482.1178.

Das, S., and C. H. Scholz (1983), Why large earthquakes do not nucleate at shallow depths, *Nature*, *305*, 621–623, doi:10.1038/305621a0.

Doser, D. I., and H. Kanamori (1986), Depth of seismicity in the Imperial Valley region (1997–1983) and its relationship to heat flow, crustal structure, and the October 15, 1979, earthquake, *J. Geophys. Res.*, *91*, 675–688, doi:10.1029/JB091iB01p00675.

Eberhart-Phillips, D., M. Lisowski, and M. D. Zoback (1990), Crustal strain near the Big Bend of the San Andreas Fault: Analysis of the Los Padres-Tehachapi trilateration networks, California, *J. Geophys. Res.*, *95*, 1139–1153, doi:10.1029/JB095iB02p01139.

Fialko, Y. (2006), Interseismic strain accumulation and the earthquake potential on the southern San Andreas Fault System, *Nature*, *441*, 968–971, doi:10.1038/nature04797.

Fuis, G. (2007), The San Andreas Fault in Southern California is almost nowhere vertical–Implications for tectonics, paper presented at the Annual Meeting of the Geological Society of America, Denver.

Fuis, G., W. Mooney, J. Healey, G. McMechan, and W. Lutter (1982), Crustal structure of the Imperial Valley region, *U.S. Geol. Surv. Prof. Pap.*, *1254*, 25–50.

Genrich, J. F., Y. Bock, and R. G. Mason (1997), Crustal deformation across the Imperial fault: Results from kinematic GPS surveys and trilateration of a densely spaced, small-aperture network, *J. Geophys. Res.*, *102*, 4985–5004, doi:10.1029/96JB02854.

Gomberg, J., J. Rubinstein, Z. Peng, K. Creager, J. Vidale, and P. Boudin (2008), Widespread triggering of nonvolcanic tremor in California, *Science*, *319*, 173, doi:10.1126/science.1149164.

Goultry, N. R., R. O. Burford, C. R. Allen, R. Gilman, C. E. Johnson, and R. P. Keller (1978), Large creep events on the Imperial fault, California, *Bull. Seismol. Soc. Am.*, *68*, 517–521.

Harris, R. A., and P. Segall (1987), Detection of a locked zone at depth on the Parkfield, California, segment on the San Andreas Fault, *J. Geophys. Res.*, *92*, 7945–7962, doi:10.1029/JB092iB08p07945.

Hill, D. P., J. P. Eaton, and L. M. Jones (1990), Seismicity, *U.S. Geol. Surv. Prof. Pap.*, *1515*, 115–151.

Lachenbruch, A., J. Sass, and S. Galanis Jr. (1985), Heat flow in southernmost California and the origin of the Salton trough, *J. Geophys. Res.*, *90*, 6709–6736, doi:10.1029/JB090iB08p06709.

Lin, G., P. M. Shearer, and E. Hauksson (2007), Applying a three-dimensional velocity model, waveform cross correlation, and cluster analysis to locate Southern California seismicity from 1981 to 2005, *J. Geophys. Res.*, *112*, B12309, doi:10.1029/2007JB004986.

Louie, J. N., C. R. Allen, D. C. Johnson, P. C. Haase, and S. N. Cohn (1985), Fault slip in Southern California, *Bull. Seismol. Soc. Am.*, *75*, 811–833.

Lyons, S., and D. Sandwell (2003), Fault creep along the southern San Andreas from interferometric synthetic aperture radar, permanent scatterers, and stacking, *J. Geophys. Res.*, *108*(B1), 2047, doi:10.1029/2002JB001831.

Lyons, S., Y. Bock, and D. T. Sandwell (2002), Creep along the Imperial fault, Southern California, from GPS measurements, *J. Geophys. Res.*, *107*(B10), 2249, doi:10.1029/2001JB000763.

Magistrale, H. (2002), Relative contributions of crustal temperature and composition to controlling the depth of earthquakes in Southern California, *Geophys. Res. Lett.*, *29*(10), 1447, doi:10.1029/2001GL014375.

Magistrale, H., and H. Zhou (1996), Lithologic control of the depth of earthquakes in Southern California, *Science*, *273*, 639–642, doi:10.1126/science.273.5275.639.

Marone, C., and C. H. Scholz (1988), The depth of seismic faulting and the upper transition from stable to unstable slip regimes, *Geophys. Res. Lett.*, *15*, 621–624, doi:10.1029/GL015i006p00621.

McCaffrey, R. (2005), Block kinematics of the Pacific–North America plate boundary in the southwestern United States from inversion of GPS, seismological, and geologic data, *J. Geophys. Res.*, *110*, B07401, doi:10.1029/2004JB003307.

Meade, B. J., and B. H. Hager (2004), Viscoelastic deformation for a clustered earthquake cycle, *Geophys. Res. Lett.*, *31*, L10610, doi:10.1029/2004GL019643.

Meade, B. J., and B. H. Hager (2005a), Block models of crustal motion in Southern California constrained by GPS measurements, *J. Geophys. Res.*, *110*, B03403, doi:10.1029/2004JB003209.

Meade, B. J., and B. H. Hager (2005b), Spatial localization of moment deficits in Southern California, *J. Geophys. Res.*, *110*, B04402, doi:10.1029/2004JB003331.

Miller, C. K., and K. P. Furlong (1988), Thermal-mechanical controls on seismicity depth distributions in the San Andreas Fault Zone, *Geophys. Res. Lett.*, *15*, 1429–1432, doi:10.1029/GL015i012p01429.

Murray, J. R., P. Segall, P. Cervelli, W. Prescott, and J. Svarc (2001), Inversion of GPS data for spatially variable slip-rate on the San Andreas Fault near Parkfield, CA, *Geophys. Res. Lett.*, *28*, 359–362, doi:10.1029/2000GL011933.

Nadeau, R. M., and D. Dolenc (2005), Nonvolcanic tremors beneath the San Andreas Fault, *Science*, *307*, 389, doi:10.1126/science.1107142.

Nazareth, J. J., and E. Hauksson (2004), The seismogenic thickness of the Southern California crust, *Bull. Seismol. Soc. Am.*, *94*, 940–960, doi:10.1785/0120020129.

Obara, K., H. Hirose, F. Yamamizu, and K. Kasahara (2004), Episodic slow slip events accompanied by nonvolcanic tremors in southwest Japan subduction zone, *Geophys. Res. Lett.*, *31*, L23602, doi:10.1029/2004GL020848.

Peterson, M. D., W. A. Bryant, C. H. Cramer, T. Cao, M. S. Reichle, A. D. Frankel, J. J. Lienkaemper, P. A. McCrory, and D. P. Schwartz (1996), Probabilistic seismic hazard assessment for the state of California, *U.S. Geol. Surv. Open File Rep. 96-76*, 1–64.

Plesch, A., and J. H. Shaw (2003), SCEC CFM: A WWW accessible community fault model for Southern California, *Eos Trans. AGU*, *84*(46), Fall Meet. Suppl., Abstract S12B-0395.

Plesch, A., et al. (2007), Community Fault Model (CFM) for Southern California, *Bull. Seismol. Soc. Am.*, *97*, 1793–1802, doi:10.1785/0120050211.

Reilinger, R., and S. Larsen (1986), Vertical crustal deformation associated with the 1979 $M = 6.6$ Imperial Valley, California, earthquake: Implications for fault behavior, *J. Geophys. Res.*, *91*, 14,044–14,056, doi:10.1029/JB091iB14p14044.

Richards-Dinger, K. B., and P. M. Shearer (2000), Earthquake locations in Southern California obtained using source-specific station terms, *J. Geophys. Res.*, *105*, 10,939–10,960, doi:10.1029/2000JB900014.

Rogers, G., and H. Dragert (2003), Episodic tremor and slip on the Cascadia Subduction Zone: The chatter of silent slip, *Science*, *300*, 1942–1943, doi:10.1126/science.1084783.

Rolandone, F., R. Bürgmann, and R. M. Nadeau (2004), The evolution of the seismic-aseismic transition during the earthquake cycle: Constraints from the time-dependent depth distribution of aftershocks, *Geophys. Res. Lett.*, *31*, L23610, doi:10.1029/2004GL021379.

Sanders, C. O. (1990), Earthquake depths and the relation to strain accumulation and stress near strike-slip faults in Southern California, *J. Geophys. Res.*, *95*, 4751–4762, doi:10.1029/JB095iB04p04751.

Savage, J. C. (1990), Equivalent strike-slip earthquake cycles in half-space and lithosphere-asthenosphere earth models, *J. Geophys. Res.*, *95*, 4873–4879, doi:10.1029/JB095iB04p04873.

Savage, J. C. (2006), Dislocation pileup as a representation of strain accumulation on a strike-slip fault, *J. Geophys. Res.*, *111*, B04405, doi:10.1029/2005JB004021.

Savage, J. C., and R. O. Burford (1973), Geodetic determination of relative plate motion in central California, *J. Geophys. Res.*, *78*, 832–845, doi:10.1029/JB078i005p00832.

Savage, J. C., and R. W. Simpson (1997), Surface strain accumulation and the seismic moment tensor, *Bull. Seismol. Soc. Am.*, *87*, 1345–1353.

Schmalzle, G., T. Dixon, R. Malservisi, and R. Govers (2006), Strain accumulation across the Carrizo segment of the San Andreas Fault, California: Impact of laterally varying crustal properties, *J. Geophys. Res.*, *111*, B05403, doi:10.1029/2005JB003843.

Segall, P. (2002), Integrating geologic and geodetic estimates of slip rate on the San Andreas Fault system, *Int. Geol. Rev.*, *44*, 62–82, doi:10.2747/0020-6814.44.1.62.

Sharp, R. V. (1981), Variable rates of late Quaternary strike slip on the San Jacinto fault zone, Southern California, *J. Geophys. Res.*, *86*, 1754–1762, doi:10.1029/JB086iB03p01754.

Shearer, P. M. (2002), Parallel fault strands at 9-km depth resolved on the Imperial fault, Southern California, *Geophys. Res. Lett.*, *29*(14), 1674, doi:10.1029/2002GL015302.

Smith, B., and D. Sandwell (2003), Coulomb stress accumulation along the San Andreas Fault System, *J. Geophys. Res.*, *108*(B6), 2296, doi:10.1029/2002JB002136.

Smith, B. R., and D. T. Sandwell (2006), A model of the earthquake cycle along the San Andreas Fault System for the past 1000 years, *J. Geophys. Res.*, *111*, B01405, doi:10.1029/2005JB003703.

Smith-Konter, B., and D. Sandwell (2009), Stress evolution of the San Andreas Fault System: Recurrence interval versus locking depth, *Geophys. Res. Lett.*, *36*, L13304, doi:10.1029/2009GL037235.

Smith-Konter, B., D. T. Sandwell, and M. Wei (2010), Integrating GPS and InSAR to resolve stressing rates of the SAF system, *EarthScope inSights Newsl., Summer 2010*, 1–3.

Stein, R. S. (2008), Appendix D: Earthquake Rate Model 2 of the 2007 Working Group for California Earthquake Probabilities, Magnitude-Area Relationships, *U.S. Geol. Surv. Open File Rep.*, *2007-1437D*, 1–16.

Thatcher, W. (1979), Systematic inversion of geodetic data in central California, *J. Geophys. Res.*, *84*, 2283–2295, doi:10.1029/JB084iB05p02283.

Vincent, P. (1998), Application of SAR interferometry to low-rate crustal deformation fields, Ph.D. dissertation, Univ. of Colo. at Boulder, Boulder, Colo.

Ward, S. N. (1994), A multidisciplinary approach to seismic hazard in Southern California, *Bull. Seismol. Soc. Am.*, *84*, 1293–1309.

Wdowinski, S. (2009), Deep creep as a cause for the excess seismicity along the San Jacinto fault, *Nat. Geosci.*, *2*, 882–885, doi:10.1038/ngeo684.

Wei, M., D. T. Sandwell, and B. Smith-Konter (2010), Optimal combination of InSAR and GPS for measuring interseismic crustal deformation, *Adv. Space Res.*, *46*, 236–249, doi:10.1016/j.asr.2010.03.013.

Weldon, R., and K. E. Sieh (1985), Holocene rate of slip and tentative recurrence interval for large earthquakes on the San Andreas Fault, Cajon Pass, Southern California, *Geol. Soc. Am. Bull.*, *96*, 793–812, doi:10.1130/0016-7606(1985)96<793:HROSAT>2.0.CO;2.

Weldon, R., T. Fumal, and G. Biasi (2004), Wrightwood and the earthquake cycle: What a long recurrence record tells us about how faults work, *GSA Today*, *14*, 4–10, doi:10.1130/1052-5173(2004)014<4:WATECW>2.0.CO;2.

Werner, C. L., P. Rosen, S. Hensley, E. Fielding, and S. Buckley (1997), Detection of aseismic creep along the San Andreas Fault near Parkfield, California, with ERS-1 radar interferometry, paper presented at the 3rd ERS Symposium, Eur. Space Agency, Florence, Italy.

Williams, C. F. (1996), Temperature and the seismic/aseismic transition: Observations from the 1992 Landers earthquake, *Geophys. Res. Lett.*, *23*, 2029–2032, doi:10.1029/96GL02066.

Working Group on California Earthquake Probabilities (WGCEP) (1995), Seismic hazards in Southern California: Probable earthquakes, 1994 to 2024, *Bull. Seismol. Soc. Am.*, *85*, 379–439.

Working Group on California Earthquake Probabilities (WGCEP) (1999), Earthquake probabilities in the San Francisco Bay Region: 2000 to 2030—A summary of findings, *U.S. Geol. Surv. Open File Rep., 99-517*, 1–60. (Available at http://geopubs.wr.usgs.gov/open-file/of99-517/.)

Working Group on California Earthquake Probabilities (WGCEP) (2003), Earthquake probabilities in the San Francisco Bay region: 2002–2031, *U.S. Geol. Surv. Open File Rep., 03-214*, 1–235. (Available at http://pubs.usgs.gov/of/2003/of03-214/.)

Working Group on California Earthquake Probabilities (WGCEP) (2007), The Uniform California Earthquake Rupture Forecast, Version 2 (UCERF 2), *U.S. Geol. Surv. Open File Rep., 2007-1473*, 1–104.

Working Group on Northern California Earthquake Potential (WGNCEP) (1996), Database of potential sources for earthquakes larger than magnitude 6 in Northern California, *U.S. Geol. Surv. Open File Rep., 96-705*.

Yule, D., and K. Sieh (2003), Complexities of the San Andreas Fault near San Gorgonio Pass: Implications for large earthquakes, *J. Geophys. Res.*, *108*(B11), 2548, doi:10.1029/2001JB000451.

D. Sandwell and P. Shearer, Institute for Geophysics and Planetary Physics, Scripps Institution of Oceanography, University of California, San Diego, 500 W. University Dr., La Jolla, CA 92093-0225, USA.

B. Smith-Konter, Department of Geological Sciences, University of Texas at El Paso, El Paso, TX 79968-0555, USA. (brkonter@utep.edu)